



CHALMERS
UNIVERSITY OF TECHNOLOGY

Vibrational Water Dynamics in Sodium-Based Prussian Blue Analogues

Downloaded from: <https://research.chalmers.se>, 2025-12-17 21:06 UTC

Citation for the original published paper (version of record):

Nielsen, I., Cheng, Y., Schwarz, F. et al (2025). Vibrational Water Dynamics in Sodium-Based Prussian Blue Analogues. *Journal of Physical Chemistry C*, 129(49): 21553-21559.
<http://dx.doi.org/10.1021/acs.jpcc.5c05783>

N.B. When citing this work, cite the original published paper.

Vibrational Water Dynamics in Sodium-Based Prussian Blue Analogues

Ida Nielsen,* Yongqiang Cheng, Fabian Schwarz, Amber Mace, Hamish Cavaye, Jeff Armstrong, Matthew G. Tucker, Maths Karlsson, William R. Brant, and Mikael S. Andersson*



Cite This: *J. Phys. Chem. C* 2025, 129, 21553–21559



Read Online

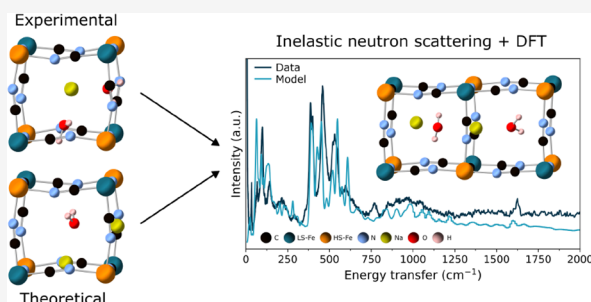
ACCESS |

Metrics & More

Article Recommendations

Supporting Information

ABSTRACT: The Prussian blue analogues (PBAs) $\text{Na}_{2-x}\text{Fe}[\text{Fe}(\text{CN})_6] \cdot z\text{H}_2\text{O}$ ($x, z = 0-2$) exhibit many phase transitions as a function of the sodium and water content, which involves large volume changes that can negatively affect its energy storage performance in a battery. However, the presence of water helps stabilize the PBA framework and thus diminishes these volume changes. To improve the material for its desired applications, a deeper fundamental understanding of the interactions between water, sodium, and the PBA framework is needed. Here, the local structure and vibrational dynamics of water were studied using inelastic neutron scattering, neutron diffraction, and theoretical calculations. When the sodium content is high, the material exhibits well-defined water environments that become less defined when the sodium content is lower. It was shown that the positions of sodium and water are more complex than suggested by previous diffraction and computational studies. Most of the water in the high sodium sample occupies the center of the PBA subcube, while only a small fraction is located close to the window site of the subcube. For the low sodium sample, the results suggest that a large distribution of local water environments is present. These results lay the groundwork for unraveling the ionic transport in PBAs and the development of improved energy storage materials.



low temperature $P2_1/n$ phase and the room temperature $R\bar{3}$ phase showed that the local structure is characterized by displacements away from the average structure, indicating dynamics of the PBA framework, sodium, and water.⁸ The sodium ordered into planes in the $P2_1/n$ phase, which consequently drove the water to obtain orientational order with the hydrogen atoms pointing away from the sodium plane. In the $R\bar{3}$ phase, the sodium was less ordered, resulting in less orientational order of the water molecules. In addition, this material exhibits anisotropic thermal expansion, which changes direction if the material is dried.⁴ This indicates that water plays a role in the phonon-driven thermal expansion as previously shown for other hydrated PBAs.⁹

1. INTRODUCTION

Sodium-based hexacyanoferrate compounds are a subgroup of Prussian blue analogues (PBAs) that have gained great interest due to their potential as positive battery electrodes, especially the compound with chemical formula $\text{Na}_{2-x}\text{Fe}[\text{Fe}(\text{CN})_6] \cdot z\text{H}_2\text{O}$ ($x, z = 0-2$).¹ The structure consists of a network of octahedrally coordinated iron atoms that are linked together via the bidentate cyanide ligands to form a porous framework which alkali cations and/or neutral guest species can occupy (Figure 1).²⁻⁴ However, the presence of water in the material greatly affects the electrochemical performance in nonaqueous battery systems, e.g., the water can react with the organic electrolyte and cause unwanted side reactions.⁵ On the other hand, water has proven to stabilize the PBA framework and thus help reduce volume changes during sodium extraction and insertion.^{6,7} To unravel the double-edged role of water, a detailed understanding of the position and dynamics of water as a function of the sodium content is needed.

Recent structural and dynamical studies of the water in $\text{Na}_2\text{Fe}[\text{Fe}(\text{CN})_6] \cdot z\text{H}_2\text{O}$ showed that during a room temperature phase transition from $P2_1/n$ to $R\bar{3}$ the ordering of the water was lost.⁴ Despite this loss of order, the localized water dynamics, consisting of water being trapped within cavities in the PBA framework, were the same in both phases.⁶ Thus, it is evident that the water has a disordered nature, hence, its local structure needs to be considered. A total scattering study of the

The experimental crystallographic data can be compared to theoretically calculated structures. However, the position of sodium within the PBA framework is still up for debate. Smaller cations, such as lithium and sodium, are thought to occupy the window sites of a PBA subcube due to their smaller size and the possibility for optimal bonding conditions when

Received: August 19, 2025
Revised: November 19, 2025
Accepted: November 25, 2025
Published: November 29, 2025



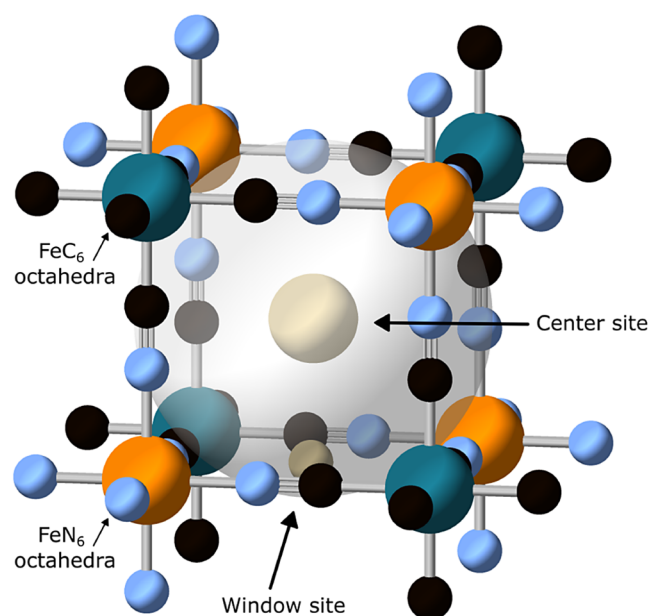


Figure 1. Basic structural arrangement in PBAs showing the porous framework built up by the iron octahedra coordinated either to carbon or nitrogen. The gray transparent sphere represents the available volume within a subcube, while the beige spheres show actual possible positions for the alkali cations and/or neutral guest species.

surrounded by the cyanide ligands (Figure 1).^{10,11} With the cation positioned on the window site, the water occupies the center of the PBA subcube. Larger cations, such as potassium, are seen to occupy the center of the PBA subcube and also limit how much water that can be present in the material due to their larger size.^{11–15} The experimentally determined average structure of $\text{Na}_2\text{Fe}[\text{Fe}(\text{CN})_6] \cdot z \text{H}_2\text{O}$ using neutron diffraction (which enables differentiating the sodium and water) showed that sodium occupies the center of the PBA subcube while water is positioned on the window sites.^{4,16} In contrast, theoretically calculated structures of sodium-based PBAs agree that the most favorable position for sodium is an off-center or window site position.^{13,14,17} The experimentally determined local structure using neutron total scattering revealed that sodium can take a wide range of positions within the PBA framework⁸ spanning the center and out to the window sites if a water molecule is not blocking its pathway. Interestingly, this discrepancy between the experimentally and theoretically determined structures is not observed when the sodium content is low.^{7,18} In summary, the sodium-based PBAs seem to be more dynamic and are therefore hard to predict based on electrostatic attractions and cation/molecular size arguments as compared to PBAs with other cations.

Since the water greatly influences the material properties in PBAs, combined with the ongoing uncertainty in where the water and sodium are positioned within the PBA framework, insight into water's interaction with the PBA framework and sodium is crucial. A method capable of probing the vibrational water dynamics is inelastic neutron scattering (INS) combined with theoretical calculations. This is because neutrons are very sensitive to hydrogen, making it possible to separate the water from the other elements present and investigate the vibrational water dynamics in PBAs as a function of the sodium content. To fully unravel the local environments for water and sodium in $\text{Na}_{2-x}\text{Fe}[\text{Fe}(\text{CN})_6] \cdot z \text{H}_2\text{O}$, further experimental data is

needed to verify the proposed structural models. Here, an INS study of PBAs with a high and low sodium and water content is presented, with the data interpreted using lattice dynamics (LD) and molecular dynamics (MD) calculations. The obtained local structure shows a dynamic system with different water and sodium positions, and that the previous perception of the positions of sodium and water within the PBA framework cannot fully describe the system.

2. METHODS

2.1. Synthesis and Sample Characterization. The as-synthesized powders were obtained from Altris AB and used as received (denoted Na2.0 and Na1.9). The sample with a low sodium content (denoted Na0.3) was made by chemically removing the sodium from the Na1.9 sample.⁶ The samples were prepared and handled in an inert atmosphere to avoid degradation. All samples were dried at 80 °C for 15 h to remove any surface water.^{6,18,19} The three samples investigated have the compositions $\text{Na}_{2.05(5)}\text{Fe}[\text{Fe}(\text{CN})_6] \cdot 2.07(2)\text{H}_2\text{O}$ (Na2.0), $\text{Na}_{1.90(9)}\text{Fe}_{0.90(7)}\text{Fe}_{0.10(3)}^{3+}[\text{Fe}^{2+}(\text{CN})_6] \cdot 2.12(2)\text{H}_2\text{O}$ (Na1.9), and $\text{Na}_{0.34(5)}\text{Fe}^{3+}[\text{Fe}^{2.66(5)+}(\text{CN})_6] \cdot 0.360(4)\text{H}_2\text{O}$ (Na0.3). Details about the sample characterization for the Na2.0 sample can be found in the Supporting Information (Tables S1–S2 and Figure S1), while the sample characterization for samples Na1.9 and Na0.3 can be found in ref 6. Thus, two samples have a high sodium content and similar water contents, while the third sample has a lower sodium and water content. The Na2.0 sample was included to exclude the effects of the minor impurity phase found in the Na1.9 sample in ref 6.

2.2. Neutron Diffraction. Variable temperature neutron diffraction data were collected on the NOMAD instrument at the Spallation Neutron Source at the Oak Ridge National Laboratory in the USA.²⁰ The Na2.0 and Na1.9 samples were packed into 6 mm cylindrical vanadium cans inside a helium-containing glovebox and sealed with copper. Data were measured at 5 and 100 K for Na2.0, and 5, 100, 200, and 300 K for Na1.9 for 1 h at each temperature. The data was reduced in the autoNOM package, with the incoherent background stemming from hydrogen being removed using a pseudo-Voigt function. The data were refined in Topas Academic V6²¹ and visualized in CrystalMaker.²² The variable temperature neutron diffraction data (Figure S2a) for the samples Na2.0 and Na1.9 down to 5 K confirm $P2_1/n$ symmetry at 5, 100, and 200 K, while the material transforms to $R\bar{3}$ symmetry at 300 K (Figure S3 and Tables S3, S4).⁸ At 5 K, the Na0.3 sample has the same symmetry ($Fm\bar{3}m$) as at room temperature, suggesting no phase transitions between 5 and 300 K (Figure S2b).⁶

2.3. Inelastic Neutron Scattering. The INS experiments were performed on the time-of-flight spectrometers TOSCA and MAPS at the ISIS Neutron and Muon Source in the UK^{23–27} and VISION at the Spallation Neutron Source at the Oak Ridge National Laboratory in the USA.²⁸ TOSCA was used to study the low frequency librational region, while MAPS was used to study the high frequency vibrations. To follow the temperature evolution of the Na1.9 sample, VISION was used due to its capability of simultaneous diffraction and INS. For the TOSCA and MAPS experiments, 1–1.5 g of sample were loaded into flat aluminum sample cans inside an argon-containing glovebox. Data were collected at 10 K for different durations depending on the water content (ca. 4 h for Na2.0

and Na1.9, and ca. 9 h for Na0.3). For the VISION experiment, 1 g of the Na1.9 and Na0.3 samples were loaded into 6 mm cylindrical vanadium cans inside a helium-containing glovebox and sealed with copper. Data were collected at 5 K for ca. 2 h. For the Na1.9 sample, data were also collected at 100, 200, and 330 K. An incident energy of 650 meV was used on MAPS, while TOSCA and VISION use a distribution of incident neutron energies. The data reduction was done using the Mantid software,²⁹ where the scattering from an empty aluminum or vanadium sample can was subtracted. For TOSCA and VISION, Q varies with the energy, while the MAPS data were integrated over $Q = 1.5\text{--}12 \text{ \AA}^{-1}$.

2.4. Computational Details. Lattice dynamics simulations by Density Functional Theory (DFT) were performed using the Vienna Ab initio Simulation Package (VASP)³⁰ to calculate INS spectra for the Na2.0 sample. The calculation used the Projector Augmented Wave (PAW) method^{31,32} to describe the effects of core electrons, with an energy cutoff of 800 eV for the plane-wave basis of the valence electrons. The lattice parameters and atomic coordinates determined in this work were used as the initial structure. The unit cell contains 44 atoms, including 4 Fe atoms. To account for the localized 3d electrons in Fe, which have two different local environments (Fe^{2+} bonding with C and Fe^{2+} bonding with N, respectively), they were assigned different Hubbard U terms, 3 eV for Fe_C^{2+} and 7 eV for Fe_N^{2+} .³³ The electronic structure was calculated on a $3 \times 2 \times 2$ Γ -centered mesh for the unit cell and at Γ point only for the $1 \times 2 \times 2$ supercell. The total energy tolerance for electronic energy minimization was 10^{-8} , and 10^{-7} eV for structure optimization. The maximum interatomic force after relaxation was below 0.002 eV/Å. The optB86b-vdW functional^{34,35} for dispersion corrections was applied. The vibrational eigenfrequencies and modes were then calculated with phonopy using the finite displacement method.³⁶ The OCLIMAX software³⁷ was used to convert the DFT-calculated phonon results to the simulated INS spectra.

Ab initio molecular dynamics (AIMD) simulations at 100 K were also performed using the $1 \times 2 \times 2$ supercell, following the canonical ensemble (NVT) implemented by Nose-Hoover thermostat. A lower cutoff energy of 500 eV and a higher total energy tolerance of 10^{-5} eV were used for faster calculations. These settings are typical for DFT molecular dynamics, which require lower accuracy than phonon calculations. The time step for the simulations was 0.2 fs, and a total of 20,000 steps were calculated for each trajectory. The trajectories were then converted to simulated INS spectra by OCLIMAX. In addition to the fully DFT-relaxed structure, constrained molecular dynamics simulations (i.e., only the water molecules were allowed to move while all other atoms were fixed at their predetermined positions) were used to understand the effect of different structure models on the INS spectra.

3. RESULTS AND DISCUSSION

3.1. General Observations of the INS Spectra. The INS spectra of the Na2.0, Na1.9, and Na0.3 samples are shown in Figure 2a. In an INS experiment on hydrogen-containing samples, the signal from hydrogen is much larger than all other elements, and thus dominates the INS spectrum.³⁸ Therefore, all peaks are assigned to the dynamics of the water molecules in the samples. The INS spectrum of a dehydrated reference sample shows only very minor contributions to the spectrum, confirming that the peaks originate from the water (Figure S4).

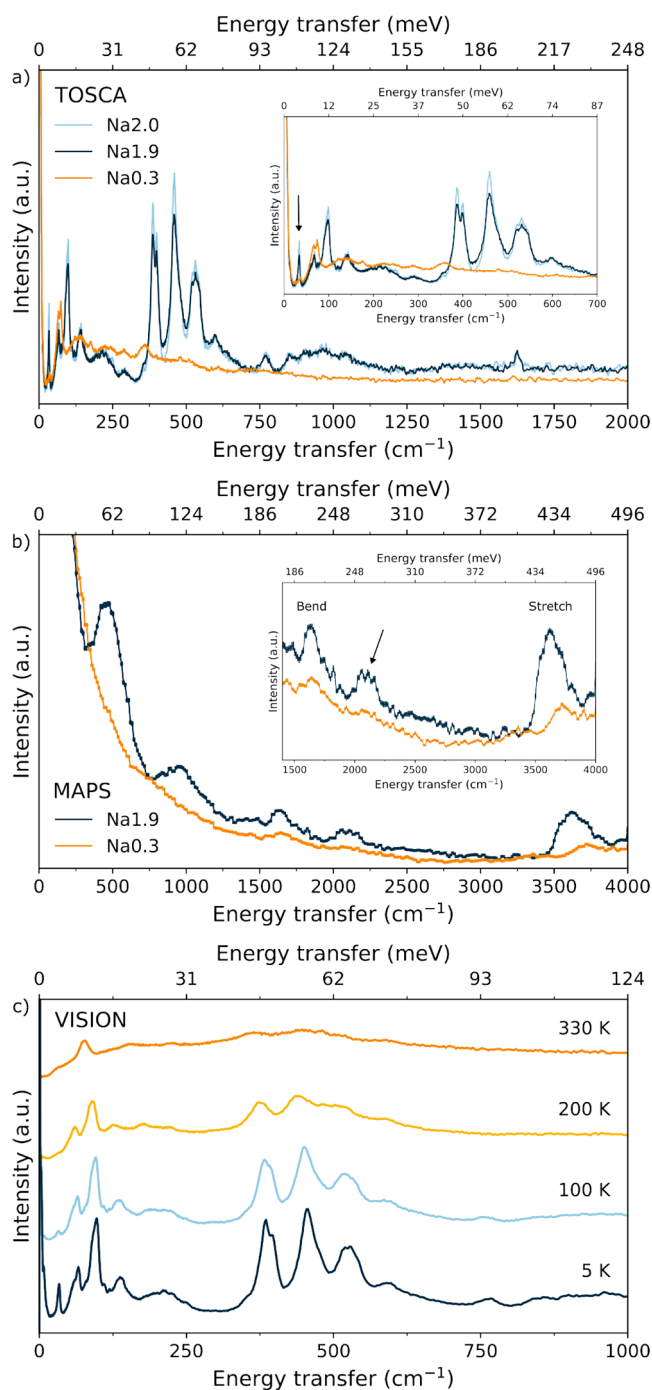


Figure 2. (a) INS spectra for the Na2.0, Na1.9, and Na0.3 samples measured on TOSCA at 10 K emphasizing the low frequency region. (b) INS spectra measured on MAPS at 10 K for samples Na1.9 and Na0.3 emphasizing the high frequency region. (c) Temperature evolution of the INS spectra measured on VISION for the Na1.9 sample.

For the two samples with a high sodium content, well-defined peaks are present. This suggests that each local water environment is well-defined, i.e., all water environments are significantly separated so that they result in sharp INS peaks rather than smeared out features. This is expected for the fully sodiated samples since the PBA framework is filled with water and sodium, creating similar local water environments throughout the structure. Below ca. 600 cm^{-1} are the librational modes, i.e., movements of the whole water

molecules without any distortions of bond lengths and angles. Comparing the spectra for the Na2.0 and Na1.9 samples, there are only minor differences. In general, the INS spectrum of the Na2.0 sample (fully sodiated) has slightly sharper peaks, possibly due to the slightly higher sodium content, and thus, a slightly smaller distribution of local water environments. The close to identical spectra for Na2.0 and Na1.9 show that the minor impurity detected in the Na1.9 sample⁶ does not affect the INS spectrum. For the sample with a low sodium content, the INS spectrum consists of broad features indicating a large distribution of local water environments throughout the structure. This is expected for the sample with a low sodium and water content since the sodium and water content within each subcube can vary due to the low occupancy.⁶ Therefore, there is more space for the water to move around, resulting in a large distribution of local water environments, which gives the broad features in the INS spectrum. In addition, the intensities of the peaks in the spectra are also reduced because of the lower water content in this sample. There is a 6% reduction of the volume during desodiation (286 \AA^3 for Na1.9 to 270 \AA^3 for Na0.3 with the subcube cell length decreasing from 5.23 \AA to 5.13 \AA), which indicates a distribution of cell volumes and subcube sizes due to the nonuniform distribution of sodium in Na0.3. This observation is in line with the broader peaks seen for the INS spectrum for Na0.3. The water-related vibrations are present at $1550\text{--}1725 \text{ cm}^{-1}$ (bend) and $3450\text{--}3850 \text{ cm}^{-1}$ (stretch) for the samples with a high sodium content (Figure 2b).³⁹ These vibrations increase in frequency to $1575\text{--}1725 \text{ cm}^{-1}$ (bend) and to $3550\text{--}3900 \text{ cm}^{-1}$ (stretch) when the sodium content is lowered due to the weaker interaction with the sodium and PBA framework. The peak at 34 cm^{-1} is present in all samples, indicating that it is related to the sodium and water content. The intensity of this peak decreases when the sodium and water content is decreased.

The temperature evolution of the INS spectrum for the Na1.9 samples was investigated since there is a phase transition at ca. 308 K.⁴ A previous quasi-elastic study suggested that the local dynamics of the water are the same in the two phases⁶ despite the water becoming disordered during the phase transition.⁴ Therefore, INS spectra were measured at 5, 100, 200, and 330 K to probe the effect of the phase transition. As the temperature increases, the INS spectra become broader due to increased thermal motion, with the peak at 98 cm^{-1} being the only peak that remains clearly visible at 330 K. The peak at 34 cm^{-1} exhibits unique temperature dependence, which diminishes quickly with increasing temperature and disappears between 100 and 200 K, suggesting a different origin from the other peaks. This peak might be related to the previously observed quantum rotational tunneling.⁶ Apart from the broadening of the spectra with temperature, no major changes are observed indicating that the water environment of the two phases is very similar, in good agreement with a previous total scattering study.⁸ However, since the features in the spectra at higher temperatures are very broad, it is hard to draw further conclusions about the phase transition from this data.

3.2. Local Coordination Environment for Water. To obtain information about the local water environments, INS spectra calculated based on different structural models were made and compared to the data. Details about the Na0.3 sample can be found in the [Supporting Information Section III A](#).

As previously discussed, there is a discrepancy between the experimentally observed structures and the theoretically calculated structures for hydrated high sodium PBA samples. Results from theoretical calculations suggest that sodium is located close to the window sites with water occupying the center, while neutron diffraction experiments suggest that the sodium is close to the center of the PBA subcube with water on the window sites.^{4,13} These two models were used as the base for the calculations of the INS spectra for the Na1.9 sample (Figures 3a,b). The calculations were performed using MD in selective dynamics mode (i.e., only the water molecules were allowed to move, while the framework and sodium were fixed) to avoid swapping of the sodium and water during structure optimization. The third model tested was a DFT-relaxed structural model containing different positions of sodium and water (Figure 3c). The INS spectrum calculated for the model with sodium at the center of the subcube (Figure 3a) describes the data poorly, especially the libration of the water in the 250 cm^{-1} region is too soft. Having sodium fixed at the center of the subcube forces the water to be closer to the window sites surrounded by the cyanide ligands. This creates an unstable position for the water as the hydrogen atoms cannot move freely or go to a desired position, and therefore, end up performing a rattling motion instead, leading to the soft librational region in the calculated spectrum. The INS spectrum calculated for the model with sodium at the window site of the subcube (Figure 3b) also describes the data poorly, however, the low frequency libration of the water is better captured in this model. The three librational peaks centered around 500 cm^{-1} in the data are also better described using this model. The INS spectrum calculated using MD for the third DFT-relaxed model containing different sodium and water positions describes the data better with more peaks assigned. For example, the peaks at ca. 300 and 1600 cm^{-1} are present in this model, whereas they are absent in the models shown in Figure 3a,b. In general, the two calculated spectra based on experimental and theoretical structures fail to describe many of the peaks in the INS data, especially at higher frequencies.

The structure in Figure 3c was fully relaxed, and therefore, LD calculations were performed (Figure 3d). Phonons in LD calculations are treated as full quantum excitations, resulting in a better match of the peak intensities relative to MD calculations. However, the peak positions are similar between the two methods (Figures 3c,d). The calculated INS spectrum shows a good agreement with the data with most features in the data described. The model with mixed sodium and water environments agrees with the observations from a previous total scattering study, which found that sodium can be positioned closer to a window site if no water molecule blocks its pathway.⁸ While the model with mixed sodium and water positions describes the data the best, it is calculated based on a cell with limited size, which may exclude some possible local configurations. However, the agreement with a total scattering study, which was carried out using big-box modeling, supports that the LD model is a good description.⁸

The LD calculation allows assignment of the INS peaks to their corresponding vibrational modes. Specifically, the group of peaks below 250 cm^{-1} is mainly due to vibrations of the water molecules, e.g., in-plane and out-of-plane rotations. Since some of these low frequency librational peaks are still present at 330 K, it suggests that the water moves similarly in the two phases. In a previous total scattering study, the water

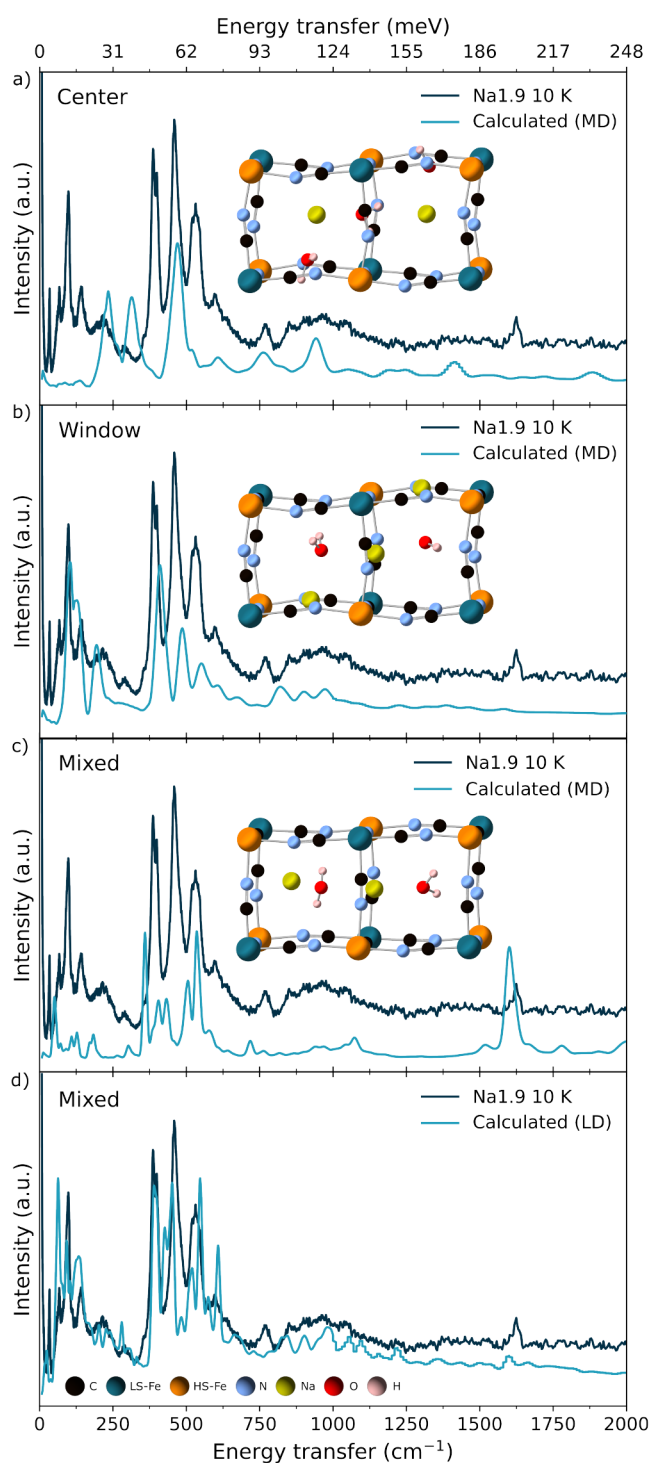


Figure 3. INS spectra calculated using MD with their corresponding structural models with sodium at (a) the center of the PBA subcube, (b) on the window site, and (c) a mixed model. (d) INS spectrum calculated using LD for the mixed model. The corresponding structural model is shown as an insert in c.

environments were also seen to be similar in two phases within a PBA subcube and at larger distances.⁸ The peaks at 350 to 600 cm^{-1} are different librational modes of the four water molecules in the unit cell and the movement of the framework. Above 605 cm^{-1} , only overtones are present (Figure S5a), except for the water bend and stretch at ca. 1600 and ca. 3600 cm^{-1} and the peaks at ca. 2100 cm^{-1} . Some overtones are also

present in the 500 cm^{-1} region. In the MAPS data (Figures 2b and S5b), peaks around 2100 cm^{-1} are present. These are due to the stretch of the cyanide ligands, which consequently causes the water molecules to move as well.⁴⁰ This confirms the strong influence of water on the thermal expansion behavior observed in these materials.⁴ Overall, the mixed model suggests that most of the water is positioned in the center of the PBA subcube (75%), allowing the water to move freely in good agreement with a previous QENS study.⁶

3.3. Refinements of the Neutron Diffraction Data Using the Mixed Model. The structural model that describes the INS data the best suggests that sodium and water can occupy different positions within the PBA framework. The LD model was therefore used to refine against the experimental neutron diffraction data for Na1.9 measured at 5 K to verify if this model can also describe the diffraction data. That is, to determine if this model is also compatible with the neutron diffraction data and if the neutron diffraction data is sensitive to distinguishing different sodium and water positions. The LD model obtained from modeling the INS data has $P1$ symmetry, which was transformed into $P2_1/n$ symmetry and then fitted to the neutron diffraction data. By applying the model, it is possible to describe most of the diffraction data by only refining the cell parameters (Figure S6 and Table S5). However, some reflections below 3.5 Å as well as the reflection at 5.8 Å are not described well. The reflections below 3.5 Å have previously been found to be related to the distortion of the iron octahedra,⁸ while the reflection at 5.8 Å corresponds to the sodium–oxygen interlayer distance.⁸ For simplicity, it was not attempted to improve the model. However, the neutron diffraction data can be acceptably described using both a model with sodium at the center of the PBA subcube (with water on the window sites) (Figure S3 and in ref 8.) and a model where the majority of the water is at the center (with most of the sodium on the window sites). Thus, the mixed model obtained from modeling the INS data can describe the neutron diffraction data. These results show that neutron diffraction (probing the average structure) alone cannot unambiguously determine the position of sodium and water in this material, and that local probes, such as INS, are appropriate tools to obtain this information.

4. CONCLUSIONS

This work covers two major questions concerning PBAs: the vibrational water dynamics in sodium-based PBAs, and the position of sodium and water within the structure of the fully sodiated PBA. To investigate these questions, INS and theoretical calculations were performed. Samples with a high sodium and water content exhibited sharp INS peaks corresponding to well-defined local water environments, while the sample with a lower sodium and water content exhibited broad spectral features due to the existence of many different local water environments. Through LD and MD calculations, it was revealed that the local structure of the high sodium sample consisted of sodium and water taking multiple positions within the PBA framework, in agreement with a previous total scattering study,⁸ and further confirming the disorder in sodium-based PBAs. The sensitivity of neutron diffraction data against the position of sodium and water was also tested, and revealed that neutron diffraction alone is not sufficient to accurately determine the structure of these PBAs. These results highlight that local structural characterization using e.g., INS is crucial and the results lay the foundation for

further computational studies, which could better explain the ionic transport in these materials.

■ ASSOCIATED CONTENT

SI Supporting Information

The Supporting Information is available free of charge at <https://pubs.acs.org/doi/10.1021/acs.jpcc.5c05783>.

Information about sample characterization, neutron diffraction data and refinements, and inelastic neutron scattering data with calculated models for high and low sodium samples (PDF)

Phonon modes obtained from the LD calculation, which can be visualized in the Jmol software (ZIP)

■ AUTHOR INFORMATION

Corresponding Authors

Ida Nielsen – Department of Chemistry - Ångström Laboratory, Uppsala University, Uppsala SE-751 21, Sweden; orcid.org/0000-0002-6511-8291; Email: ida.nielsen@kemi.uu.se

Mikael S. Andersson – Department of Chemistry - Ångström Laboratory, Uppsala University, Uppsala SE-751 21, Sweden; orcid.org/0000-0002-7119-0951; Email: mikael.andersson@kemi.uu.se

Authors

Yongqiang Cheng – Neutron Science Division, Oak Ridge National Laboratory, Oak Ridge, Tennessee 37831, United States; orcid.org/0000-0002-3263-4812

Fabian Schwarz – Department of Chemistry - Ångström Laboratory, Uppsala University, Uppsala SE-751 21, Sweden; orcid.org/0000-0002-6798-3182

Amber Mace – Department of Chemistry - Ångström Laboratory, Uppsala University, Uppsala SE-751 21, Sweden; orcid.org/0000-0002-0323-0210

Hamish Cavaye – ISIS Pulsed Neutron and Muon Source, STFC Rutherford Appleton Laboratory, Didcot OX11 0QX, U.K.; orcid.org/0000-0002-3540-0253

Jeff Armstrong – ISIS Pulsed Neutron and Muon Source, STFC Rutherford Appleton Laboratory, Didcot OX11 0QX, U.K.; orcid.org/0000-0002-8326-3097

Matthew G. Tucker – Neutron Science Division, Oak Ridge National Laboratory, Oak Ridge, Tennessee 37831, United States; orcid.org/0000-0002-2891-7086

Maths Karlsson – Department of Chemistry and Chemical Engineering, Chalmers University of Technology, Göteborg SE-412 96, Sweden; orcid.org/0000-0002-2914-6332

William R. Brant – Department of Chemistry - Ångström Laboratory, Uppsala University, Uppsala SE-751 21, Sweden

Complete contact information is available at:

<https://pubs.acs.org/doi/10.1021/acs.jpcc.5c05783>

Author Contributions

I.N.: Conceptualization, validation, formal analysis, investigation, data curation, writing—original draft, writing—review & editing, visualization, project administration. Y.C.: Methodology, validation, data curation, writing—review & editing. F.S.: Methodology, validation, data curation, writing—review & editing. A.M.: Supervision. H.C.: Investigation, resources, data curation, writing—review & editing. J.A.: Investigation, resources, data curation, writing—review & editing. M.G.T.: Resources, data curation, supervision, writing—review &

editing. M.K.: Conceptualization, writing—review & editing, supervision. W.R.B.: Conceptualization, validation, resources, writing—review & editing, supervision, funding acquisition. M.S.A.: Conceptualization, validation, investigation, data curation, writing—review & editing, supervision, project administration.

Notes

The authors declare the following competing financial interest(s): W.R.B. is a co-founder of the company Altris AB, which produces Prussian white powder for sodium-ion battery applications.

■ ACKNOWLEDGMENTS

This research is funded by Stiftelsen för Strategisk Forskning (SSF) within the Swedish National Graduate School in Neutron Scattering, SwedNess (GSn15-0008). W.R.B. acknowledges funding from the Strategic Research Area StandUp for Energy and Energimyndigheten (45517-1). M.S.A. acknowledges support from the ÅForsk Foundation grant no. 21-453 and the Göran Gustafsson Foundation. We gratefully acknowledge the Science and Technology Facilities Council (STFC) for access to neutron beamtime at ISIS, and also for the provision of sample preparation, at the TOSCA (RB2310259) and MAPS (RB2310257) facilities. Gustav Ek is acknowledged for his assistance during the INS beamtimes. This research used resources at the Spallation Neutron Source, a DOE Office of Science User Facility operated by the Oak Ridge National Laboratory. The beamtime was allocated to VISION on proposal number IPTS-34846.1 and to NOMAD on proposal number IPTS-31723.1. This research used computing resources made available through the VirtuES and the ICE-MAN projects, funded by the Laboratory Directed Research and Development program and Compute and Data Environment for Science (CADES) at ORNL, as well as resources of the National Energy Research Scientific Computing Center (NERSC), a U.S. Department of Energy Office of Science User Facility located at Lawrence Berkeley National Laboratory, operated under Contract No. DE-AC02-05CH11231 using NERSC award ERCAP0024340. Wei Zhou is acknowledged for the initial discussion of the data and modeling. Alexandra Ulander is acknowledged for performing the synthesis of the Na_{0.3} sample, and the Mössbauer experiment and analysis.

■ REFERENCES

- (1) Brant, W. R.; Mogensen, R.; Colbin, S.; Ojwang, D. O.; Schmid, S.; Häggström, L.; Ericsson, T.; Jaworski, A.; Pell, A. J.; Younesi, R. Selective Control of Composition in Prussian White for Enhanced Material Properties. *Chem. Mater.* **2019**, *31*, 7203–7211.
- (2) Wang, B.; Han, Y.; Wang, X.; Bahlawane, N.; Pan, H.; Yan, M.; Jiang, Y. Prussian Blue Analogs for Rechargeable Batteries. *iScience* **2018**, *3*, 110–133.
- (3) Chen, J.; Wei, L.; Mahmood, A.; Pei, Z.; Zhou, Z.; Chen, X.; Chen, Y. Prussian blue, its analogues and their derived materials for electrochemical energy storage and conversion. *Energy Storage Mater.* **2020**, *25*, 585–612.
- (4) Nielsen, I.; Dzodan, D.; Ojwang, D. O.; Henry, P. F.; Ulander, A.; Ek, G.; Häggström, L.; Ericsson, T.; Boström, H. L. B.; Brant, W. R. Water driven phase transitions in Prussian White cathode materials. *J. Phys. Energy* **2022**, *4*, No. 044012.
- (5) Rudola, A.; Du, K.; Balaya, P. Monoclinic Sodium Iron Hexacyanoferrate Cathode and Non-Flammable Glyme-Based Electrolyte for Inexpensive Sodium-Ion Batteries. *J. Electrochem. Soc.* **2017**, *164*, A1098–A1109.

- (6) Nielsen, I.; Ulander, A.; Juranyi, F.; Larsen, S. R.; Karlsson, M.; Brant, W. R.; Andersson, M. S. Impact of Sodium on the Water Dynamics in Prussian Blue Analogues. *Chem. Mater.* **2024**, *36*, 11246–11253.
- (7) Guo, X.; Wang, Z.; Deng, Z.; Li, X.; Wang, B.; Chen, X.; Ong, S. P. Water Contributes to Higher Energy Density and Cycling Stability of Prussian Blue Analogue Cathodes for Aqueous Sodium-Ion Batteries. *Chem. Mater.* **2019**, *31*, 5933–5942.
- (8) Nielsen, I.; Eremenko, M.; Zhang, Y.; Tucker, M. G.; Brant, W. R. Local structure of hydrated and dehydrated Prussian white cathode materials. *J. Mater. Chem. C* **2025**, *1*.
- (9) Goodwin, A. L.; Chapman, K. W.; Kepert, C. J. Guest-dependent negative thermal expansion in nanoporous prussian blue analogues $M^{\text{II}}\text{Pt}^{\text{IV}}(\text{CN})_6 \cdot x\text{H}_2\text{O}$ ($0 \leq x \leq 2$; $M = \text{Zn}, \text{Cd}$). *J. Am. Chem. Soc.* **2005**, *127*, 17980–17981.
- (10) Boström, H. L. B.; Brant, W. R. Octahedral tilting in Prussian blue analogues. *J. Mater. Chem. C* **2022**, *10*, 13690–13699.
- (11) Hegner, F. S.; Galán-Mascarós, J. R.; López, N. A Database of the Structural and Electronic Properties of Prussian Blue, Prussian White, and Berlin Green Compounds through Density Functional Theory. *Inorg. Chem.* **2016**, *55*, 12851–12862.
- (12) Deng, L.; Qu, J.; Niu, X.; Liu, J.; Zhang, J.; Hong, Y.; Feng, M.; Wang, J.; Hu, M.; Zeng, L.; et al. Defect-free potassium manganese hexacyanoferrate cathode material for high-performance potassium-ion batteries. *Nat. Commun.* **2021**, *12*, 2167.
- (13) Ling, C.; Chen, J.; Mizuno, F. First-principles study of alkali and alkaline earth ion intercalation in iron hexacyanoferrate: The important role of ionic radius. *J. Phys. Chem. C* **2013**, *117*, 21158–21165.
- (14) Liu, S.; Smith, K. C. Effects of interstitial water and alkali cations on the expansion, intercalation potential, and orbital coupling of nickel hexacyanoferrate from first principles. *J. Appl. Phys.* **2022**, *131*, 105101.
- (15) Cattermull, J.; Pasta, M.; Goodwin, A. L. Structural complexity in Prussian blue analogues. *Mater. Horiz.* **2021**, *8*, 3178–3186.
- (16) Song, J.; Wang, L.; Lu, Y.; Liu, J.; Guo, B.; Xiao, P.; Lee, J. J.; Yang, X. Q.; Henkelman, G.; Goodenough, J. B. Removal of Interstitial H_2O in Hexacyanometallates for a Superior Cathode of a Sodium-Ion Battery. *J. Am. Chem. Soc.* **2015**, *137*, 2658–2664.
- (17) Xiao, P.; Song, J.; Wang, L.; Goodenough, J. B.; Henkelman, G. Theoretical study of the structural evolution of a $\text{Na}_2\text{FeMn}(\text{CN})_6$ Cathode upon Na Intercalation. *Chem. Mater.* **2015**, *27*, 3763–3768.
- (18) Ojwang, D. O.; Häggström, L.; Ericsson, T.; Angström, J.; Brant, W. R. Influence of sodium content on the thermal behavior of low vacancy Prussian white cathode material. *Dalt. Trans.* **2020**, *49*, 3570–3579.
- (19) Ojwang, D. O.; Häggström, L.; Ericsson, T.; Mogensen, R.; Brant, W. R. Guest water hinders sodium-ion diffusion in low-defect Berlin green cathode material. *Dalt. Trans. Adv. Artic.* **2022**, *51*, 14712–14720.
- (20) Neufeind, J.; Feygenson, M.; Carruth, J.; Hoffmann, R.; Chipley, K. K. The Nanoscale Ordered MAterials Diffractometer NOMAD at the Spallation Neutron Source SNS. *Nucl. Instruments Methods Phys. Res. Sect. B Beam Interact. with Mater. Atoms* **2012**, *287*, 68–75.
- (21) Coelho, A. A. TOPAS and TOPAS-Academic: An optimization program integrating computer algebra and crystallographic objects written in C++. *J. Appl. Crystallogr.* **2018**, *51*, 210–218.
- (22) *Images and video generated using CrystalMaker®: a crystal and molecular structures program for Mac and Windows.* CrystalMaker Software Ltd: Oxford, England. www.crystallmaker.com.
- (23) Ewings, R. A.; Stewart, J. R.; Perring, T. G.; Bewley, R. I.; Le, M. D.; Raspino, D.; Pooley, D. E.; Skoro, G.; Waller, S. P.; Zacek, D.; et al. Upgrade to the MAPS neutron time-of-flight chopper spectrometer. *Rev. Sci. Instrum.* **2019**, *90*, No. 035110.
- (24) Parker, S. F.; Carlile, C. J.; Pike, T.; Tomkinson, J.; Newport, R. J.; Andreani, C.; Ricci, F. P.; Sacchetti, F.; Zoppi, M. TOSCA: a world class inelastic neutron spectrometer. *Phys. B Condens. Matter* **1997**, *241–243*, 154–156.
- (25) Parker, S. F.; Fernandez-Alonso, F.; Ramirez-Cuesta, A. J.; Tomkinson, J.; Rudic, S.; Pinna, R. S.; Gorini, G.; Fernández Castañón, J. Recent and future developments on TOSCA at ISIS. *J. Phys. Conf. Ser.* **2014**, *554*, No. 012003.
- (26) Andersson, M. S.; Ek, G.; Brant, W. R.; Nielsen, I.; Karlsson, M.; Cavaye, H. *Inelastic neutron scattering on Prussian White as a function of the Na and water content*, 2024.
- (27) Andersson, M. S.; Ek, G.; Brant, W. R.; Nielsen, I.; Karlsson, M.; Armstrong, J. *Inelastic neutron scattering on Prussian White as a function of the Na and water content*. 2024; .
- (28) Seeger, P. A.; Daemen, L. L.; Larese, J. Z. Resolution of VISION, a crystal-analyzer spectrometer. *Nucl. Instruments Methods Phys. Res. Sect. A Accel. Spectrometers, Detect. Assoc. Equip.* **2009**, *604*, 719–728.
- (29) Arnold, O.; Bilheux, J. C.; Borreguero, J. M.; Buts, A.; Campbell, S. I.; Chapon, L.; Doucet, M.; Draper, N.; Ferraz Leal, R.; Gigg, M. A.; et al. Mantid - Data analysis and visualization package for neutron scattering and μ SR experiments. *Nucl. Instruments Methods Phys. Res. Sect. A Accel. Spectrometers, Detect. Assoc. Equip.* **2014**, *764*, 156–166.
- (30) Kresse, G.; Furthmüller, J. Efficient iterative schemes for ab initio total-energy calculations using a plane-wave basis set. *Phys. Rev. B* **1996**, *54*, 11169–11186.
- (31) Blöchl, P. E. Projector augmented-wave method. *Phys. Rev. B* **1994**, *50*, 17953–17979.
- (32) Kresse, G.; Joubert, D. From ultrasoft pseudopotentials to the projector augmented-wave method. *Phys. Rev. B* **1999**, *59*, 1758–1775.
- (33) Wojdel, J. C.; Moreira, I. d. P. R.; Bromley, S. T.; Illas, F. On the prediction of the crystal and electronic structure of mixed-valence materials by periodic density functional calculations: The case of Prussian Blue. *J. Chem. Phys.* **2008**, *128*, No. 044713.
- (34) Perdew, J. P.; Ernzerhof, M.; Burke, K. Rationale for mixing exact exchange with density functional approximations. *J. Chem. Phys.* **1996**, *105*, 9982–9985.
- (35) Klimeš, J.; Bowler, D. R.; Michaelides, A. Chemical accuracy for the van der Waals density functional. *J. Phys.: Condens. Matter* **2010**, *22*, No. 022201.
- (36) Togo, A.; Tanaka, I. First principles phonon calculations in materials science. *Scripta Materialia* **2015**, *108*, 1–5.
- (37) Cheng, Y. Q.; Kolesnikov, A. I.; Ramirez-Cuesta, A. J. Simulation of Inelastic Neutron Scattering Spectra Directly from Molecular Dynamics Trajectories. *J. Chem. Theory Comput.* **2020**, *16*, 7702–7708.
- (38) Parker, S. F.; Lennon, D.; Albers, P. W. Vibrational spectroscopy with neutrons: A review of new directions. *Appl. Spectrosc.* **2011**, *65*, 1325–1341.
- (39) Perakis, F.; Marco, L. D.; Shalit, A.; Tang, F.; Kann, Z. R.; Kühne, T. D.; Torre, R.; Bonn, M.; Nagata, Y. Vibrational Spectroscopy and Dynamics of Water. *Chem. Rev.* **2016**, *116*, 7590–7607.
- (40) Kettle, S. F.; Diana, E.; Aschero, G. L.; Diana, E.; Rossetti, R.; Stanghellini, P. L. The vibrational spectra of the cyanide ligand revisited: Terminal cyanides. *Inorg. Chem.* **2006**, *45*, 4928–4937.